2mif

NASA TECHNICAL NOTE

NASA TN D-7466

NASA TN D-7466

EFFECTS OF MACH NUMBER ON PITOT-PROBE DISPLACEMENT IN A TURBULENT BOUNDARY LAYER

by Jerry M. Allen

Langley Research Center
Hampton, Va. 23665

NATIONAL AERONAUTICS AND SPACE ADMINISTRATION • WASHINGTON, D. C. • JUNE 1974

1. Report No.	2. Government Accession No.	3. Recipient's Catalog No.
NASA TN D-7466		

4. Title and Subtitle	5. Report Date
EFFECTS OF MACH NUMBER ON PITOT-PROBE DISPLACEMENT IN A TURBULENT BOUNDARY LAYER	June 1974
	6. Performing Organization Code
7. Author(s)	8. Performing Organization Report No.
Jerry M. Allen	L-9253
	10. Work Unit No.
9. Performing Organization Name and Address	760-65-03-01
NASA Langley Research Center Hampton, Va. 23665	11. Contract or Grant No.
	13. Type of Report and Period Covered
12. Sponsoring Agency Name and Address	Technical Note
National Aeronautics and Space Administration Washington, D.C. 20546	14. Sponsoring Agency Code

15. Supplementary Notes

16. Abstract

Experimental pitot-probe-displacement data have been obtained in a turbulent boundary layer at a local free-stream Mach number of 4.63 and unit Reynolds number of 6.46×10^6 per meter. The results of this study were compared with lower Mach number results of previous studies. It was found that small probes showed displacement only, whereas the larger probes showed not only displacement but also distortion of the shape of the boundary-layer profile. The distortion pattern occurred lower in the boundary layer at the higher Mach number than at the lower Mach number. The maximum distortion occurred when the center of the probe was about one probe diameter off the test surface. For probes in the wall contact position, the indicated Mach numbers were, for all probes tested, close to the true profile. Pitot-probe displacement was found to increase significantly with increasing Mach number.

17. Key Words (Suggested by Author(s))	18. Distribution Statement
Turbulent boundary layer Pitot-probe displacement Supersonic flow	Unclassified – Unlimited STAR Category 12

19. Security Classif. (of this report)	20. Security Classif. (of this page)	21. No. of Pages	22. Price*
Unclassified	Unclassified	~~33~~ 36	$3.25

*For sale by the National Technical Information Service, Springfield, Virginia 22151

EFFECTS OF MACH NUMBER ON PITOT-PROBE DISPLACEMENT IN A TURBULENT BOUNDARY LAYER

By Jerry M. Allen
Langley Research Center

SUMMARY

Experimental pitot-probe-displacement data have been obtained in a turbulent boundary layer at a local free-stream Mach number of 4.63 and unit Reynolds number of 6.46×10^6 per meter. The results of this study are compared with lower Mach number results of previous studies. It is found that smaller probes show displacement only, whereas the larger probes showed displacement as well as distortion of the shape of the boundary-layer profile. The distortion pattern at the higher Mach number occurred lower in the boundary layer than the pattern at the lower Mach number. The maximum distortion occurred when the center of the probe was about one probe diameter off the test surface. For probes in the wall-contact position, the indicated Mach numbers were, for all probes tested, close to the true Mach number. Pitot-probe displacement was found to increase significantly with increasing Mach number.

INTRODUCTION

When a pitot probe is placed in a shear-gradient flow, the probe does not measure the true pressure that existed at the center of the probe in the undisturbed stream. The effective center of the probe is thus said to be "displaced" from the geometric center. Corrections to measured profiles can be made for this effect, however, if the magnitude and direction of the displacement are known. The introduction of reference 1 contains a summary of previous experimental and theoretical work on this subject. The results of reference 1 indicated that the pitot-probe displacement in a Mach 2 turbulent boundary layer was about twice as large as had been previously obtained in incompressible turbulent boundary layers. It was not known, however, if this displacement is a gradual Mach number effect or merely a "supersonic" effect; that is, a step effect caused by the bow shock that exists ahead of the probe in supersonic flow. Data at a high supersonic Mach number should resolve this question. This study was thus conducted to provide pitot-probe displacement data in a turbulent boundary layer at a free-stream Mach number of 4.6, and to assess the trends of pitot probe displacement with Mach number.

SYMBOLS

U.S. Customary Units were employed for the experimental measurements in this study, but the International System of Units (SI) is used herein to report the results.

D	external diameter of circular pitot probe or external height of flattened pitot probe
d	internal diameter of circular pitot probe
l_{eq}	equivalent flat-plate length
M	Mach number
N	power-law velocity-profile exponent
p	pressure
R	unit Reynolds number, $\rho u/\mu$
T	temperature
u	velocity in streamwise direction
y	normal coordinate (see fig. 1)
γ	ratio of specific heats (1.4 for air)
Δ	mean pitot-probe displacement derived from figures 5 and 6
δ	boundary-layer total thickness
δ^*	boundary-layer displacement thickness (see eq. (8))
θ	boundary-layer momentum thickness (see eq. (7))
μ	viscosity
ρ	density

Subscripts:

aw	adiabatic wall
e	boundary-layer edge
m	measured by pitot probe
0	evaluated at $D = 0$
t	stagnation
w	wall
∞	free stream

APPARATUS AND TESTS

Wind Tunnel

The experimental data contained in this study were obtained in the high-speed test section of the Langley Unitary Plan wind tunnel, which is described in reference 2. This variable-pressure, continuous-flow tunnel has a two-dimensional asymmetric sliding-block nozzle that permits a continous variation in the test-section Mach number from about 2.3 to 4.6. The normal operating stagnation temperature is between 339 K and 352 K. The test section is about 1.22 meters wide by 1.22 meters high by 2.13 meters long.

Test Station

The tunnel sidewall was used as the model in this investigation. The turbulent boundary layer on the sidewall was surveyed on the sidewall center line about midway of the test section. The boundary layer at the survey station for the test conditions of this study was about 150 mm thick. The equivalent flat-plate length (that is, the length of turbulent flat-plate flow at the same free-stream conditions of the survey station needed to produce the same boundary layer) to the survey station was about 8.7 meters.

The top and bottom walls of the tunnel are contoured to produce the supersonic flow. The sidewalls, one of which was used as the test surface, are flat from the nozzle throat to the downstream edge of the test section.

Instrumentation

The tunnel sidewall boundary layer was surveyed with nine pitot probes ranging in size from 0.26 mm to 48 mm (0.2 to 32 percent of the boundary-layer thickness). These probes are the same as those used in reference 1 to obtain the displacement results at Mach 2. Because of the large displacement trends obtained in reference 1, questions were raised as to the possible effects of probe geometry on the measured profiles. Hence, subsequent to completion of the present tests, check runs were performed at Mach 2 to investigate the effects of probe tip and support geometry. The small flattened probe, a flat-ended circular probe, and a beveled probe (with a 29° included cone angle) were tested with circular and diamond-shaped support shafts so that the effects of bevel angle and support configuration could be separated. Neither of these parameters was found to have any measurable effect on the displacement results and consequently these data are not presented herein.

The smallest probe used in the present investigation was a conventional flattened boundary-layer probe (fig. 1), and was used to provide a reference survey of the boundary layer. The remaining eight probes were circular, with ratios of inside diameter to outside diameter of about 0.6. These probes were used to obtain the displacement data. These probes, as can be seen from the sketch in figure 1, were double-ended; that is, two probes were mounted back-to-back on a single shaft. In this configuration, data from two probes could be recorded without the necessity of a tunnel shutdown, probe change, and subsequent tunnel restart. This procedure allowed the tunnel running time to be cut approximately in half. Insulating tape was applied to the tunnel wall in the area immediately downstream of the shaft to insure that the contact light would be activated only when the upstream probe touched the wall.

The double-ended probe was mounted on a shaft which ran through the tunnel sidewall. An O-ring seal was used between the shaft and the sidewall to eliminate leakage. Probe position normal to the wall was controlled manually from outside the tunnel by a traversing mechanism connected to the probe shaft. The surface location was determined by electrical contact between the wall and the probe tip, and the position above the test surface was determined from the surface contact point and a dial indicator connected to the probe shaft. The dial indicator could be set to within about 0.003 mm.

Pitot-probe pressures were measured by a pressure transducer having a range of 0 to 0.2 atmosphere and a normal accuracy of about 0.25 percent of its full-scale reading. Tunnel stagnation pressures were measured by a precision automatic indicating mercury manometer. All data were recorded on punched cards for data reduction purposes.

Tests and Procedures

The test was conducted at a nominal free-stream Mach number of 4.6 and stagnation pressure of 2.46 atmospheres. Tunnel stagnation temperature was maintained at about 352 K so that the wall temperature would be close enough to the ambient temperature outside the test section to insure that no appreciable temperature gradients were present across the tunnel wall. Hence, this test was run near zero heat-transfer conditions. These test conditions resulted in a free-stream unit Reynolds number of about 6.56×10^6 per meter. The tunnel dewpoint was maintained at about 244 K.

The boundary layer at the test station was surveyed by each of the probes in turn. The test procedure consisted of bringing the probe in contact with the tunnel wall, as determined by the contact light, and then moving the probe away from the wall in small increments, and recording data. The probes were positioned so that all probes had their centers at the same locations across the boundary layer. A complete boundary-layer survey by each probe took about 30 minutes.

DATA REDUCTION

Mach Number

The pitot pressure measured by the small reference probe outside the boundary layer $p_{m,e}$ and the measured tunnel stagnation pressure $p_{t,\infty}$ were used to calculate the local free-stream Mach number by the normal-shock relation

$$\frac{p_{m,e}}{p_{t,\infty}} = \left[\frac{(\gamma + 1)M_e^2}{(\gamma - 1)M_e^2 + 2}\right]^{\frac{\gamma}{\gamma-1}} \left(\frac{\gamma + 1}{2\gamma M_e^2 - \gamma + 1}\right)^{\frac{1}{\gamma-1}} \tag{1}$$

This Mach number and $p_{m,e}$ value were then used to calculate the static pressure at the boundary-layer edge p_e from the Rayleigh pitot formula

$$\frac{p_{m,e}}{p_e} = \left[\frac{(\gamma + 1)M_e^2}{2}\right]^{\frac{\gamma}{\gamma-1}} \left(\frac{\gamma + 1}{2\gamma M_e^2 - \gamma + 1}\right)^{\frac{1}{\gamma-1}} \tag{2}$$

The static pressure was then assumed to be constant through the boundary layer and equal to the calculated edge value. The Mach number distributions through the boundary layer were then calculated from the measured p_m and calculated p_e values. If p_m/p_e was greater than 1.893, the supersonic Mach numbers were calculated by equation (2) in

which local conditions replace the boundary-layer edge conditions. If p_m/p_e was less than 1.893, the subsonic Mach numbers were calculated from the isentropic flow equation

$$\frac{p_m}{p_e} = \left(1 + \frac{\gamma - 1}{2} M^2\right)^{\frac{\gamma}{\gamma-1}} \tag{3}$$

Velocity Ratio

Velocity ratios are related to Mach number and temperature by

$$\frac{u}{u_e} = \frac{M}{M_e}\sqrt{\frac{T}{T_t}}\sqrt{\frac{T_{t,e}}{T_e}}\sqrt{\frac{T_t}{T_{t,e}}} \tag{4}$$

where

$$\left.\begin{aligned} \frac{T_t}{T} &= 1 + \frac{\gamma - 1}{2} M^2 \\ \frac{T_{t,e}}{T_e} &= 1 + \frac{\gamma - 1}{2} M_e^2 \end{aligned}\right\} \tag{5}$$

Inserting equations (5) into equation (4) and assuming isoenergetic flow $\left(T_t = T_{t,e}\right)$ results in

$$\frac{u}{u_e} = \frac{M}{M_e}\sqrt{\frac{1 + \frac{\gamma - 1}{2} M_e^2}{1 + \frac{\gamma - 1}{2} M^2}} \tag{6}$$

which was used to calculate velocity ratios herein.

Integral Thicknesses

Boundary-layer momentum thickness θ and displacement thickness δ^* are defined in two-dimensional compressible flow to be

$$\theta = \int_0^{\delta} \frac{\rho u}{\rho_e u_e}\left(1 - \frac{u}{u_e}\right)dy \tag{7}$$

and

$$\delta^* = \int_0^{\delta}\left(1 - \frac{\rho u}{\rho_e u_e}\right)dy \tag{8}$$

If the assumptions of constant static pressure and total temperature across the boundary layer are used, the density ratio ρ/ρ_e can be written as

$$\frac{\rho}{\rho_e} = \frac{T_e}{T} = \frac{1 + \frac{\gamma - 1}{2} M^2}{1 + \frac{\gamma - 1}{2} M_e{}^2} \tag{9}$$

Equations (6) and (9) allow the calculation of the integrands in equations (7) and (8) for each data point in the boundary layer. The integrations were performed by parabolic curve fitting through successive data points and stepwise integration of the resulting curves.

RESULTS AND DISCUSSION

Probe-Size Effects

Probe-displacement effects are evaluated in this study in terms of Mach number values calculated from the measured pressures. These Mach number values are shown in figure 2 as a function of probe diameter (nondimensionalized with respect to boundary-layer thickness δ) with the curves connecting points of constant y/δ; that is, points whose probe centers are located at the same position in the boundary layer. The solid symbols indicate points where the probes were touching the test surface.

Data for y/δ values greater than 0.872 were omitted from figure 2 for clarity. These data would simply fair into the M_e value when the probes were outside the boundary layer. Note that some of the indicated Mach numbers for the larger probes at large y/δ values are greater than the true boundary-layer edge value – a phenomenon termed "overshoot." This phenomenon has been reported previously in a turbulent boundary layer (ref. 1), a laminar boundary layer (ref. 3), and wakes (refs. 4 and 5), but all have been in supersonic flow with large probes relative to the wake or boundary-layer size. It is difficult to understand this phenomenon except in terms of a nonnormal shock. Since normal-

shock relations are used in data reduction, any flow passing through an inclined shock could give indicated Mach numbers which are larger than the free-stream value.

Note that the smallest probe size for which data are plotted in figure 2 is the flattened reference probe, which was used to help substantiate the small-probe Mach number trends. A circular probe with a diameter equal to the height of the flattened probe could not have been used because of the prohibitive lag time and viscous effects resulting from the very small diameter.

For the smaller probe diameters, the variation of indicated Mach number with probe diameter appears to be linear. Thus, as was done in reference 6 for incompressible flow and in reference 1 for Mach 2 flow, linear extrapolations through the data for small-diameter probes were performed to obtain the true Mach number profile for this boundary layer, which is defined as the profile for $D = 0$.

Note that the Mach numbers for the wall contact points (solid symbols in fig. 2) are close to the true Mach number at that value of y/δ. This trend was noted also in the lower Mach number results of reference 1 and indicates that Preston tube data contain negligible displacement effects throughout the supersonic Mach number range. The kinks in the curves at the larger probe diameters result from extreme distortion of the indicated boundary-layer profile, probably as a result of boundary-layer separation upstream of the larger probes. This phenomenon was noted in reference 1 for Mach 2 flow. The largest probe used in the present study was about 32 percent of the boundary-layer thickness, whereas it was about 70 percent in reference 1. Comparing figure 2 with figure 3 of reference 1 reveals that at similar values of D/δ, the distortion pattern of the present data occurs in a lower part of the boundary layer than the pattern of reference 1. The present results therefore do not contain overshoot as extensive as that contained in the lower Mach number data, and the reasons for the overshoot appear to be different. In reference 1, where the distortion occurs in the outer part of the boundary layer, the overshoot is simply a part of the distortion region, whereas in the present results, where the distortion occurs lower in the boundary layer, the small amount of overshoot is not a part of the distortion region. If the distortion trend in the present data continues for larger values of D/δ, then D/δ values even larger than those reached in reference 1 would be required at this higher Mach number to produce distortion near the boundary-layer edge, and hence an extensive overshoot pattern.

True Profile

The result of the linear extrapolation of the small-probe-diameter data of figure 2 to $D = 0$ is the true Mach number profile, which is shown in figure 3(a). The profile shape below $\frac{y}{\delta} = 0.034$ is the same as the flattened-probe profile since figure 2 shows

that no linear extrapolation could be performed at these low values of y/δ. The smooth variation of Mach number through the boundary layer shown in figure 3(a) gives confidence in the linear extrapolations.

These Mach number values, converted to velocity ratio u/u_e, are shown plotted in log-log form in figure 3(b). The linear variation of velocity ratio with y/δ in this plot shows that this true profile follows a normal turbulent-boundary-layer power-law form, and that the power-law exponent N of this profile is about 10.9. The integration of this true profile yielded a momentum thickness θ of 4.77 mm and a displacement thickness δ^* of 49.9 mm. The boundary-layer total thickness was estimated to be about 150 mm.

Measured Profiles Compared With True Profile

The profiles measured by each of the nine probes and a comparison with the true profile are shown in figures 4(a) to 4(i). The flattened reference probe profile (fig. 4(a)) is in very good agreement with the true profile as would be expected from figure 2. The results from flattened probes, which are of the type normally used in boundary-layer research, generally do not require displacement corrections since the probe dimension in the direction of the velocity gradient is small.

Figures 4(b) to 4(i) show the profiles from the eight circular probes, increasing in size from $\frac{D}{\delta} = 0.009$ in figure 4(b) to $\frac{D}{\delta} = 0.322$ in figure 4(i). The indicated Mach number values are generally larger than the true value at the same value of y/δ – an indication of positive displacement. This trend increases with increasing probe size.

Since there should be no probe displacement in zero-shear flow, Mach number profiles from all probes should equal the local free-stream value when the probe is entirely outside the boundary layer; that is, at about half the probe diameter above the boundary-layer edge. Hence, the Mach number profiles for the probes of larger diameters asymptotically approach the true profile at values of y/δ somewhat greater than 1. For the probes of smaller diameter, the experimental profiles in the local free stream are within about 0.2 percent of the true-profile value.

Beginning with the $\frac{D}{\delta} = 0.068$ profile (fig. 4(d)), a kink appears in the profiles in the lower part of the boundary layer. This kink increases in severity and moves farther away from the test surface with the increasing probe size, a trend which was noted also in the lower Mach number results of reference 1. The peak of the kinks in the present results and in those of reference 1 occurs at y/D values of about 1; that is, the maximum distortion at both Mach numbers (and boundary-layer thicknesses) occurs when the center of the probe is about one probe diameter off the test surface. As mentioned previously, this distortion of the indicated Mach number profile, which is superimposed on the normal

probe displacement effects, is probably caused by separation of the boundary layer upstream of the larger probes when they are in close proximity to the test surface.

Note, however, that, regardless of the severity of the distortion and displacement of the probes as they traverse the boundary layer, when they are in the wall contact position, that is, acting as Preston tubes, the indicated Mach numbers are close to the true value at that y/δ. This trend explains why valid Preston tube results were obtained in reference 7 even with large probes.

Tabulated values of the Mach number and velocity ratio are presented in tables I to III.

Probe-Displacement Calculations

Probe displacement is, by definition, the distance that the measured profile would need to be displaced to agree with the true profile. The direct method, then, of obtaining probe-displacement results would be to measure the vertical distance between the symbols and curve in figure 4. Reference 1 reported, however, that an equivalent method of making these measurements for small-diameter probes can be obtained from the slopes of the curves of Mach number plotted as a function of diameter and the slopes of the true Mach number profile. The resulting equation is

$$\frac{\Delta}{D} = \left.\frac{\partial \bar{M}/\partial \bar{D}}{\partial M/\partial y}\right|_0$$

This method is used to obtain the displacement results presented herein. The $\left.\frac{\partial M}{\partial D}\right|_0$ values were obtained from the slopes of the linear extrapolations of figure 2, and the $\left.\frac{\partial M}{\partial y}\right|_0$ values were obtained from the slopes of the true profiles as seen in figure 3(a).

The $\left.\frac{\partial M}{\partial D}\right|_0$ distribution is shown in figure 5. There is some scatter in these slopes, but the overall trend is clear. The solid curve represents a fairing of the data.

The $\left.\frac{\partial M}{\partial y}\right|_0$ distribution is shown in figure 6. The data scatter is much less here as compared with that of figure 5, but a faired curve was put through the data for consistency.

The displacement distribution was then obtained by dividing the faired curve of figure 5 by the faired curve of figure 6, and the results are shown in figure 7. Shown for

comparison are the $M_e = 1.975$ results of reference 1, in which the derivative trends were faired to give a smoother displacement trend, and unpublished results at $M_e = 2.125$ which were obtained by the present author in support of the results of reference 1. The incompressible-flow results of reference 6 are shown also on this figure.

The displacement results near the boundary-layer edge are noted to be very inaccurate and are therefore ignored in the process of estimating trends herein. Intuitively, it can be reasoned that since the displacement in zero-shear flow should be zero, the displacement distributions should smoothly fair to zero in the free stream and the fairing should be gradual and not abrupt. In practice, however, it is very difficult to estimate accurately the displacement trends in this region by either the direct-measurement technique or the slope-calculation technique. The direct-measurement technique has difficulty, as reported in reference 1, because of the small Mach number gradients near the boundary-layer edge. The slope-calculation technique encounters difficulty because the faired curves of both $\left.\frac{\partial M}{\partial D}\right|_0$ and $\left.\frac{\partial M}{\partial y}\right|_0$ approach zero near the boundary-layer edge so that their division produces highly inaccurate numbers in this region. Hence, the very inaccurate data in figure 7 are identified with solid symbols. The trend to inaccuracy, however, is gradual, so that even the open symbols at the higher values of y/δ are not as accurate as those farther down in the boundary layer. The gradual dropoff to zero displacement at the boundary-layer edge, therefore, cannot be determined from the present data.

Effect of Mach Number on Probe Displacement

The major objective of this investigation is to assess the Mach number trends in probe displacement. Figure 7 shows a large effect of Mach number on displacement. Not only is the level of the present results much larger than those at the lower Mach numbers, but the displacement distribution increases through the high Mach number boundary layer, a trend which did not appear at the lower Mach numbers. The increasing values of displacement through the boundary layer at $M_e = 4.63$ can be explained in terms of Mach number since the local Mach number increases through the boundary layer.

This trend would not be present in the incompressible-flow results of reference 6 because of the very low Mach number. It is not known why this trend was not present in the $M_e = 1.975$ and 2.125 results, but it should be noted that the difference in Mach number across the boundary layer for the data shown in figure 7 is about 0.8 for the lower Mach number data, whereas it is about 2.6 for the higher Mach number data. Thus, any Mach number trend would be more apparent in the present results.

Figure 8 shows the data of figure 7 plotted against local Mach number. There appears to be a fairly smooth trend of displacement with Mach number. The faired curve

in figure 8 is therefore presented tentatively as the effect of Mach number on pitot-probe displacement in a turbulent boundary layer.

SUMMARY OF RESULTS

Experimental pitot-probe displacement data have been obtained in a turbulent boundary layer at a local free-stream Mach number of 4.63 and unit Reynolds number of 6.46×10^6 per meter. Comparing the results of this study with the lower Mach number results of previous studies has yielded the following conclusions:

1. The pattern of small probes showing displacement and of large probes showing displacement as well as distortion which was observed at lower supersonic Mach numbers was also obtained in the present study.

2. For similar values of probe size to boundary-layer thickness, the high Mach number data showed a distortion pattern which was lower in the boundary layer than the pattern at the lower Mach number.

3. When distortion occurred, the maximum distortion occurred when the center of the probe was about one probe diameter off the test surface.

4. For probes in the wall contact position, the indicated Mach numbers were, for all probes tested, close to the true profile.

5. Pitot-probe displacement was found to increase significantly with increasing Mach number.

Langley Research Center,
National Aeronautics and Space Administration,
Hampton, Va., March 25, 1974.

REFERENCES

1. Allen, Jerry M.: Pitot-Probe Displacement in a Supersonic Turbulent Boundary Layer. NASA TN D-6759, 1972.

2. Schaefer, William T., Jr.: Characteristics of Major Active Wind Tunnels at the Langley Research Center. NASA TM X-1130, 1965.

3. Davies, F. V.: Some Effects of Pitot Size on the Measurement of Boundary Layers in Supersonic Flow. Tech. Note No. Aero. 2179, Brit. R.A.E., Aug. 1952.

4. Johannesen, N. H.; and Mair, W. A.: Experiments With Large Pitot Tubes in a Narrow Supersonic Wake. J. Aeronaut. Sci., vol. 19, no. 11, Nov. 1952, pp. 785-787.

5. Marson, G. B.; and Lilley, G. M.: The Displacement Effect of Pitot Tubes in Narrow Wakes at Subsonic and Supersonic Speeds. Rep. No. 107, Coll. of Aeronaut., Cranfield (Engl.), Oct. 1956.

6. MacMillan, F. A.: Experiments on Pitot-Tubes in Shear Flow. R. & M. No. 3028, Brit. A.R.C., 1957.

7. Allen, Jerry M.: Evaluation of Compressible-Flow Preston Tube Calibrations. NASA TN D-7190, 1973.

TABLE I.- TRUE PROFILE

$[M_e = 4.630;\ R_e = 6.46 \times 10^6/\text{m};\ T_t = 352\ \text{K};\ \theta = 4.77\ \text{mm};\ \delta^* = 49.9\ \text{mm};\ \delta = 150\ \text{mm};\ \frac{T_w}{T_{aw}} \approx 1;\ N = 10.9;\ l_{eq} = 8.7\ \text{m}]$

y/δ	M	u/u_e
0.001	0.469	0.228
.004	.924	.424
.008	1.339	.571
.034	1.880	.715
.059	2.115	.763
.085	2.275	.793
.110	2.418	.816
.135	2.553	.836
.161	2.665	.851
.186	2.770	.865
.212	2.855	.875
.237	2.937	.884
.262	3.040	.895
.288	3.128	.904
.313	3.208	.912
.339	3.268	.919
.364	3.365	.926
.415	3.518	.938
.441	3.584	.943
.466	3.662	.948
.491	3.720	.952
.516	3.792	.957

y/δ	M	u/u_e
0.542	3.846	0.961
.567	3.928	.966
.593	3.978	.969
.618	4.024	.971
.643	4.100	.976
.669	4.142	.978
.694	4.208	.981
.720	4.265	.984
.745	4.323	.987
.770	4.368	.989
.796	4.405	.991
.821	4.445	.993
.847	4.482	.994
.872	4.520	.996
.897	4.543	.997
.923	4.567	.998
.948	4.582	.999
.974	4.595	.999
.999	4.603	1.000
1.024	4.614	1.000
1.050	4.620	1.000

TABLE II.- MACH NUMBER AND VELOCITY PROFILES FOR FLATTENED REFERENCE PROBE

y/δ	M	u/u_e
0.001	0.469	0.228
.004	.924	.424
.008	1.339	.571
.034	1.871	.713
.059	2.099	.760
.085	2.281	.793
.110	2.431	.817
.135	2.560	.836
.161	2.669	.851
.220	2.891	.878
.271	3.068	.898
.322	3.244	.914
.373	3.405	.928
.423	3.542	.939
0.474	3.692	.950
.525	3.822	.959
.576	3.928	.965
.627	4.060	.973
.677	4.183	.979
.728	4.292	.985
.779	4.395	.990
.830	4.467	.993
.881	4.528	.996
.931	4.572	.998
.982	4.597	.999
1.033	4.611	.999
1.041	4.612	.999

TABLE III.- MACH NUMBER AND VELOCITY PROFILES FOR CIRCULAR PROBES

(a) $D/\delta = 0.009$

y/δ	M	u/u_e
0.004	1.138	0.504
.008	1.120	.498
.034	1.808	.698
.059	2.058	.752
.085	2.226	.784
.110	2.378	.809
.135	2.516	.830
.161	2.645	.848
.186	2.749	.862
.212	2.852	.874
.237	2.949	.885
.262	3.039	.895
.288	3.130	.904
.313	3.213	.912
.339	3.290	.919
.364	3.370	.925
.389	3.446	.932
.415	3.530	.938
.441	3.594	.943
.466	3.670	.948
.491	3.732	.953
.516	3.800	.958
.542	3.871	.962
.567	3.925	.965
.593	3.986	.969
.618	4.046	.972
.643	4.111	.975
.669	4.170	.979
.694	4.229	.982
.720	4.279	.984
.745	4.338	.987
.770	4.383	.989
.796	4.431	.991
.821	4.459	.993
.847	4.500	.995
.872	4.533	.996
.897	4.557	.997
.923	4.580	.998
.948	4.595	.999
.974	4.606	.999
.999	4.618	1.000
1.024	4.623	1.000
1.050	4.625	1.000

(b) $D/\delta = 0.016$

y/δ	M	u/u_e
	----	----
0.008	1.396	0.588
.034	1.978	.736
.059	2.179	.775
.085	2.333	.802
.110	2.485	.823
.135	2.595	.841
.161	2.709	.856
.186	2.815	.870
.212	2.912	.881
.237	2.980	.888
.262	3.098	.900
.288	3.179	.908
.313	3.250	.915
.339	3.333	.922
.364	3.403	.928
.389	3.480	.934
.415	3.559	.940
.441	3.620	.945
.466	3.692	.950
.491	3.779	.956
.516	3.843	.960
.542	3.891	.963
.567	3.938	.966
.593	4.016	.970
.618	4.066	.973
.643	4.139	.977
.669	4.175	.979
.694	4.249	.983
.720	4.293	.985
.745	4.355	.988
.770	4.392	.990
.796	4.444	.992
.821	4.473	.993
.847	4.511	.995
.872	4.534	.996
.897	4.560	.997
.923	4.579	.998
.948	4.594	.999
.974	4.602	.999
.999	4.612	.999
1.024	4.619	1.000

(c) $D/\delta = 0.068$

y/δ	M	u/u_e
0.034	1.879	0.714
.042	2.118	.764
.051	2.271	.791
.059	2.379	.809
.068	2.429	.817
.076	2.459	.822
.085	2.478	.824
.093	2.523	.831
.102	2.549	.835
.110	2.604	.843
.135	2.711	.857
.161	2.828	.871
.186	2.935	.883
.212	3.032	.894
.237	3.129	.904
.262	3.215	.912
.288	3.301	.919
.313	3.372	.926
.339	3.535	.939
.364	3.535	.939
.389	3.621	.945
.415	3.696	.950
.441	3.764	.955
.466	3.834	.959
.491	3.903	.964
.516	3.959	.967
.542	4.027	.971
.567	4.083	.974
.593	4.141	.977
.618	4.200	.980
.643	4.253	.983
.669	4.305	.986
.694	4.374	.989
.720	4.413	.991
.745	4.457	.993
.770	4.505	.995
.796	4.543	.996
.821	4.561	.997
.847	4.583	.998
.872	4.599	.999
.897	4.612	.999
.923	4.620	1.000
.948	4.627	1.000
.974	4.623	1.000
.999	4.627	1.000
1.024	4.633	1.000

(d) $D/\delta = 0.119$

y/δ	M	u/u_e
0.059	2.085	0.757
.085	2.547	.835
.093	2.647	.848
.102	2.725	.859
.110	2.763	.863
.119	2.768	.864
.127	2.763	.863
.135	2.756	.862
.144	2.787	.866
.152	2.822	.870
.161	2.853	.874
.186	2.944	.884
.212	3.035	.894
.237	3.149	.905
.262	3.224	.913
.288	3.333	.922
.313	3.411	.929
.339	3.482	.934
.364	3.558	.940
.389	3.636	.946
.415	3.710	.951
.441	3.784	.956
.466	3.856	.961
.491	3.921	.965
.516	3.995	.969
.542	4.042	.972
.567	4.107	.975
.593	4.165	.978
.618	4.229	.982
.643	4.292	.985
.669	4.359	.988
.694	4.410	.991
.720	4.465	.993
.745	4.491	.994
.770	4.541	.996
.796	4.573	.998
.821	4.608	.999
.847	4.635	1.000
.872	4.646	1.001
.897	4.659	1.001
.923	4.661	1.001
.948	4.611	1.001
.974	4.660	1.001
1.024	4.652	1.001

(e) $D/\delta = 0.169$

y/δ	M	u/u_e
0.085	2.302	0.797
.110	2.700	.855
.135	2.985	.889
.161	3.081	.899
.186	3.050	.896
.212	3.114	.902
.237	3.205	.911
.262	3.297	.919
.288	3.378	.926
.313	3.467	.933
.339	3.548	.940
.364	3.613	.944
.389	3.706	.951
.415	3.756	.954
.441	3.838	.960
.466	3.903	.964
.491	3.973	.968
.516	4.029	.971
.542	4.083	.974
.567	4.147	.978
.593	4.208	.981
.618	4.260	.983
.643	4.337	.987
.669	4.377	.989
.694	4.439	.992
.720	4.473	.993
.745	4.529	.996
.770	4.558	.997
.796	4.601	.999
.821	4.620	1.000
.847	4.652	1.001
.872	4.668	1.002
.897	4.675	1.002
.923	4.676	1.002
.948	4.680	1.002
.974	4.672	1.002
.999	4.665	1.001
1.024	4.660	1.001
1.050	4.653	1.001

(f) $D/\delta = 0.220$

y/δ	M	u/u_e
0.110	2.450	0.820
.135	2.778	.865
.161	3.072	.898
.186	3.301	.920
.212	3.341	.923
.237	3.296	.919
.262	3.353	.924
.288	3.421	.930
.313	3.512	.937
.339	3.590	.943
.364	3.667	.948
.389	3.737	.953
.415	3.822	.959
.441	3.888	.963
.466	3.956	.967
.491	4.013	.970
.516	4.072	.973
.542	4.147	.978
.567	4.201	.980
.593	4.255	.983
.618	4.322	.986
.643	4.372	.989
.669	4.427	.991
.694	4.475	.993
.720	4.536	.996
.745	4.579	.998
.770	4.611	.999
.796	4.647	1.001
.821	4.670	1.002
.847	4.689	1.002
.872	4.701	1.003
.897	4.715	1.003
.923	4.716	1.003
.948	4.710	1.003
.974	4.704	1.003
.999	4.696	1.003
1.024	4.694	1.003

(g) $D/\delta = 0.271$

y/δ	M	u/u_e
0.135	2.565	0.837
.161	2.856	.874
.186	3.109	.901
.212	3.361	.925
.220	3.416	.929
.237	3.547	.939
.262	3.544	.940
.279	3.672	.949
.288	3.715	.952
.313	3.552	.940
.296	3.742	.953
.339	3.613	.944
.305	3.733	.953
.364	3.688	.950
.313	3.705	.951
.389	3.773	.955
.339	3.646	.947
.415	3.848	.960
.364	3.693	.950
.441	3.907	.964
.389	3.754	.954
.466	3.978	.968
.415	3.836	.959
.491	4.043	.972
.441	3.889	.963
.516	4.107	.975
.466	3.949	.966
.542	4.159	.979
.491	4.020	.971
.567	4.220	.981
.516	4.089	.974
.593	4.275	.984
.542	4.145	.977
.618	4.343	.987
.567	4.209	.981
.643	4.399	.990
.593	4.269	.984
.669	4.453	.992
.618	4.318	.986
.694	4.504	.995
.643	4.403	.990
.720	4.551	.997
.669	4.455	.993
.745	4.600	.999
.694	4.505	.995
.770	4.627	1.000
.720	4.568	.997
.796	4.674	1.002
.745	4.600	.999
.821	4.701	1.003
.770	4.642	1.001
.847	4.724	1.004
.796	4.681	1.002
.872	4.729	1.004
.821	4.706	1.003
.897	4.742	1.005
.847	4.724	1.004
.921	4.743	1.005
.872	4.735	1.004
.948	4.738	1.004
.897	4.750	1.005
.974	4.732	1.004
.923	4.714	1.004
.999	4.722	1.004
.948	4.747	1.005
1.024	4.697	1.003
.974	4.736	1.004
1.050	4.696	1.003
.999	4.727	1.004
1.075	4.685	1.002
1.024	4.713	1.003
1.101	4.682	1.002
1.050	4.705	1.003
1.126	4.678	1.002
1.075	4.698	1.003
1.135	4.675	1.002
1.101	4.683	1.002
1.109	4.683	1.002

(h) $D/\delta = 0.322$

y/δ	M	u/u_e
0.161	2.607	0.843
.186	2.852	.874
.212	3.096	.900
.237	3.304	.920
.262	3.533	.939
.271	3.605	.944
.279	3.672	.949
.288	3.715	.952
.296	3.742	.953
.305	3.733	.953
.313	3.705	.951
.339	3.646	.947
.364	3.693	.950
.389	3.754	.954
.415	3.836	.959
.441	3.889	.963
.466	3.949	.966
.491	4.020	.971
.516	4.089	.974
.542	4.145	.977
.567	4.209	.981
.593	4.269	.984
.618	4.318	.986
.643	4.403	.990
.669	4.455	.993
.694	4.505	.995
.720	4.568	.997
.745	4.600	.999
.770	4.642	1.001
.796	4.681	1.002
.821	4.706	1.003
.847	4.724	1.004
.872	4.735	1.004
.897	4.750	1.005
.923	4.714	1.004
.948	4.747	1.005
.974	4.736	1.004
.999	4.727	1.004
1.024	4.713	1.003
1.050	4.705	1.003
1.075	4.698	1.003
1.101	4.683	1.002
1.109	4.683	1.002

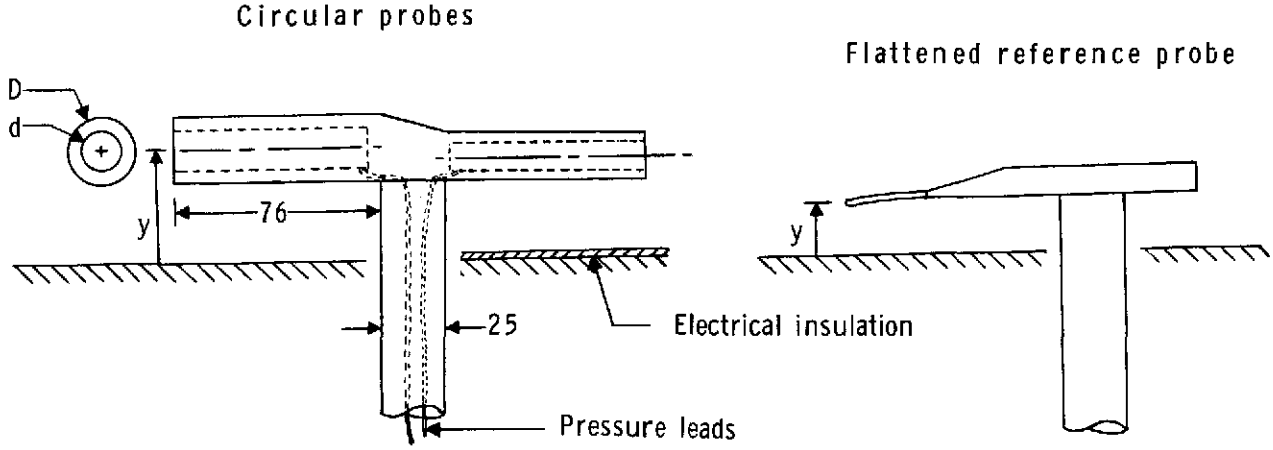

Probe diameters

Probe	d	D	d/D
1	0.76	1.27	.60
2	1.40	2.38	.59
3	6.10	10.2	.60
4	10.7	17.8	.60
5	15.2	25.4	.60
6	19.8	33.0	.60
7	24.4	40.6	.60
8	29.0	48.3	.60

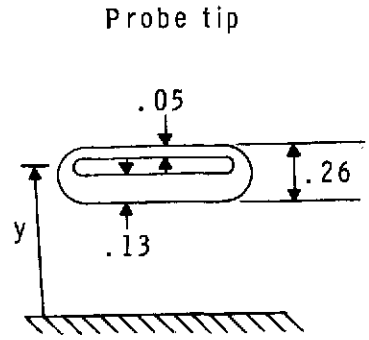

Figure 1.- Probe sketches. All dimensions are in millimeters.

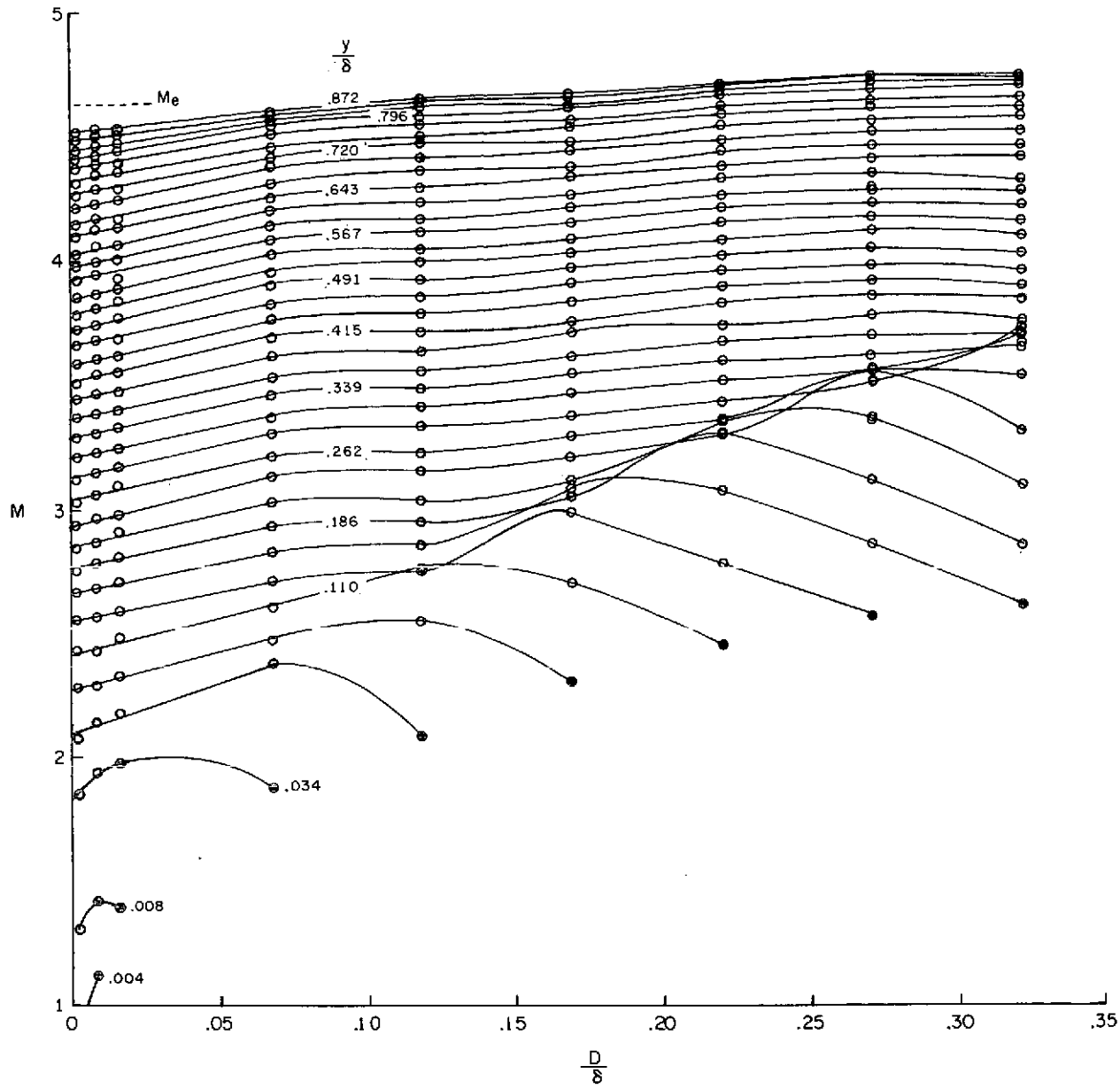

Figure 2.- Effect of probe size on measured Mach number. Solid symbols indicate wall contact points.

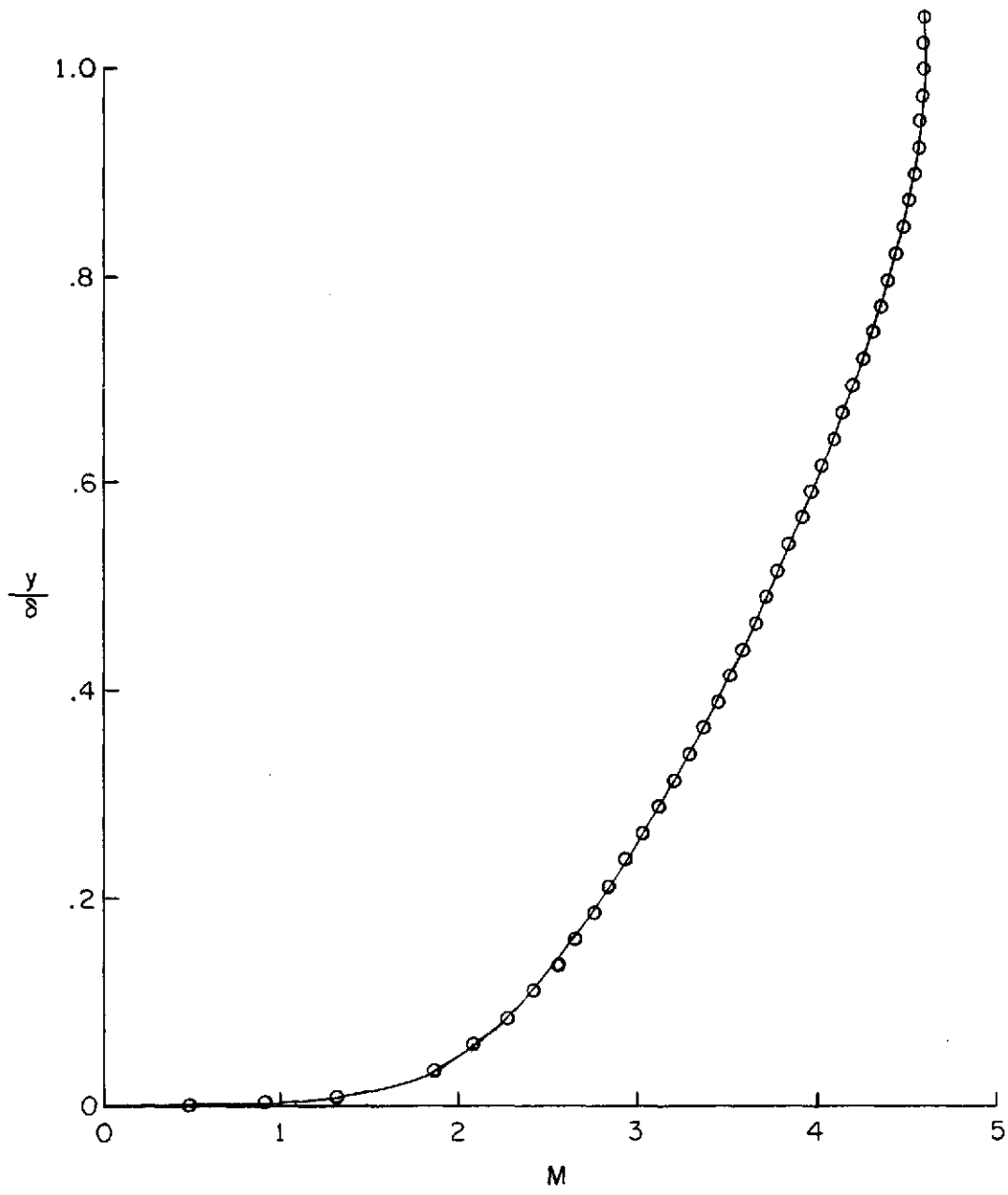

(a) Mach number profile.

Figure 3.- True profile.

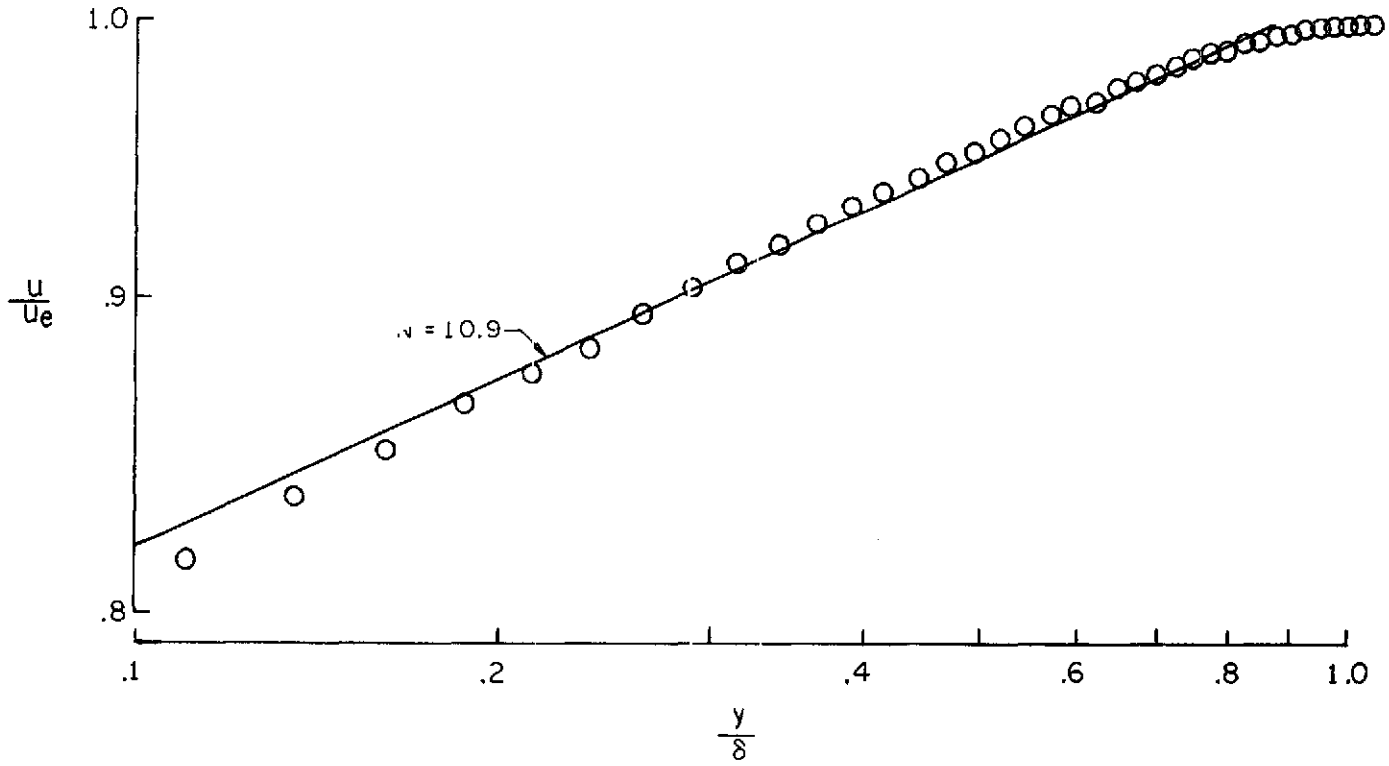

(b) Velocity profile.

Figure 3.- Concluded.

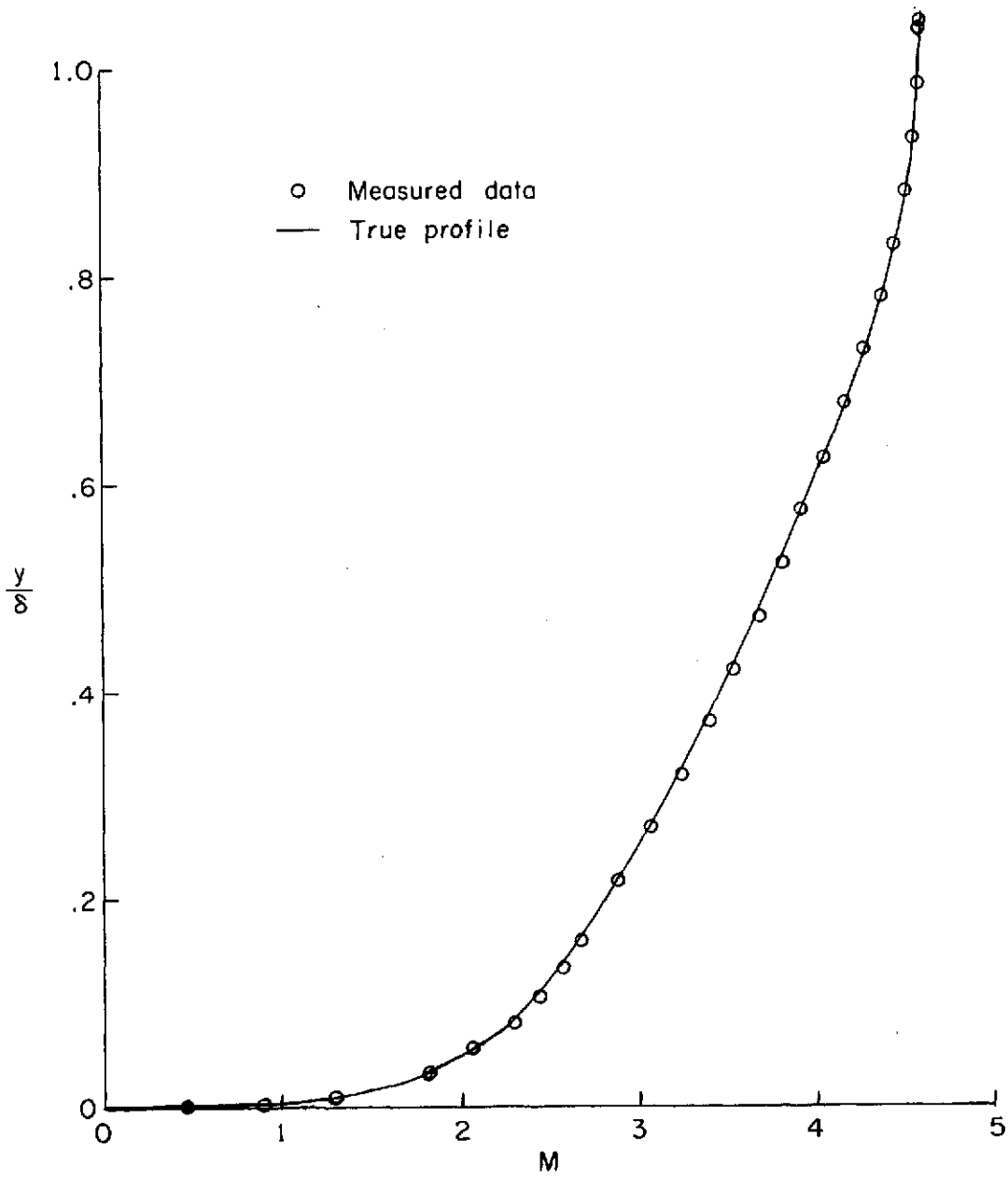

(a) Flattened reference probe. Solid symbol indicates wall contact point.

Figure 4.- Measured profiles compared with true profile.

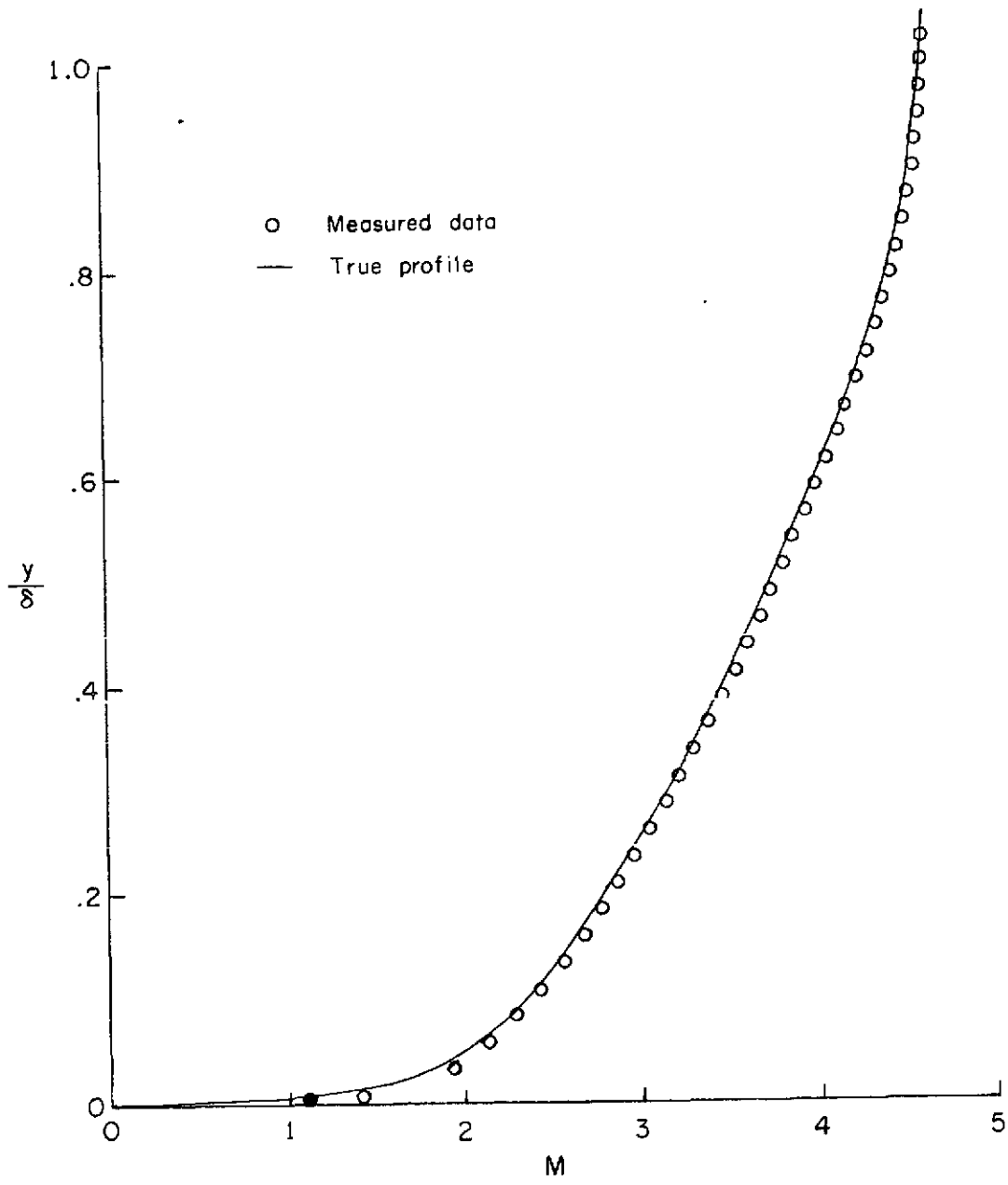

(b) $\frac{D}{\delta} = 0.009$. Solid symbol indicates wall contact point.

Figure 4.- Continued.

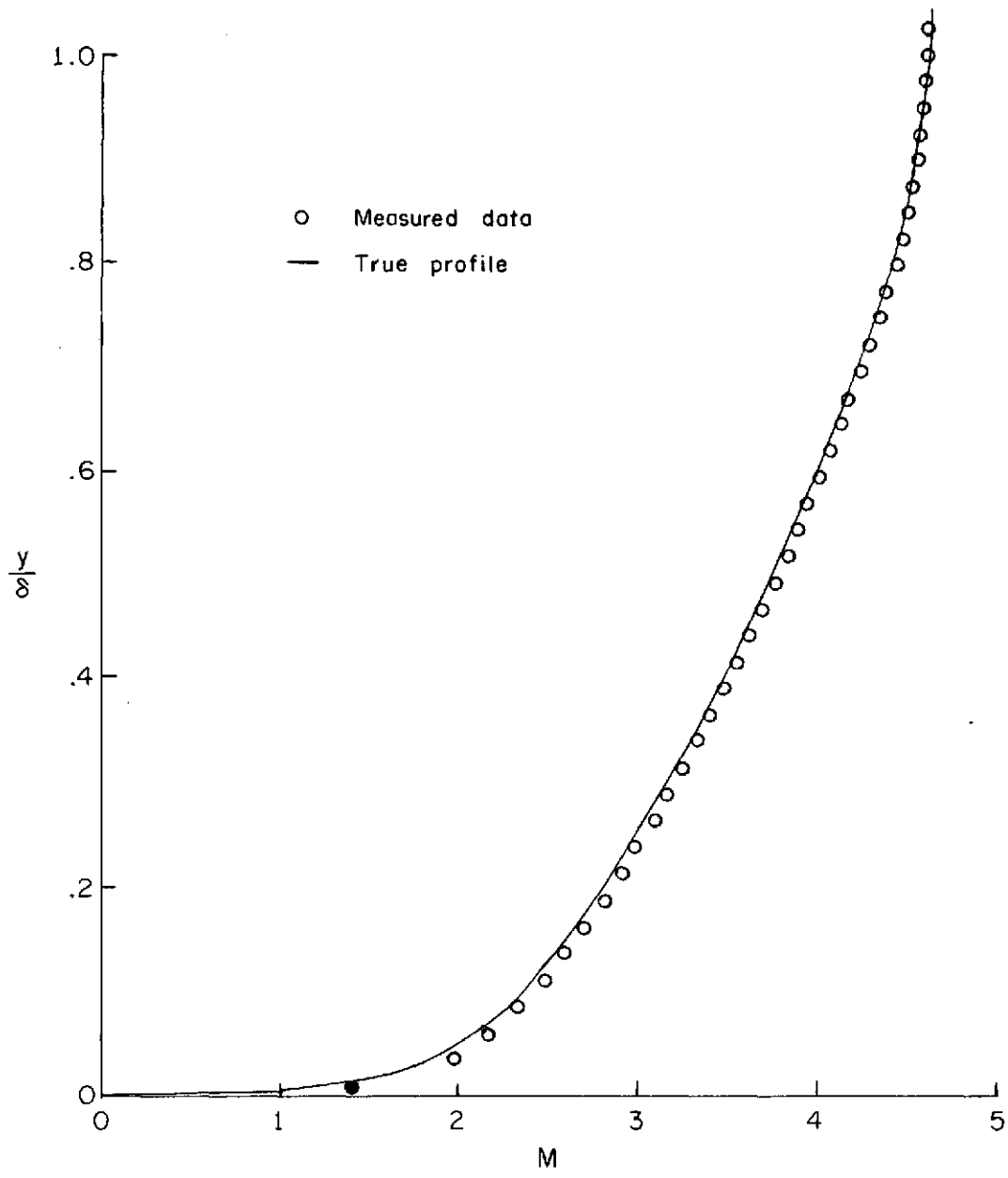

(c) $\frac{D}{\delta} = 0.016$. Solid symbol indicates wall contact point.

Figure 4.- Continued.

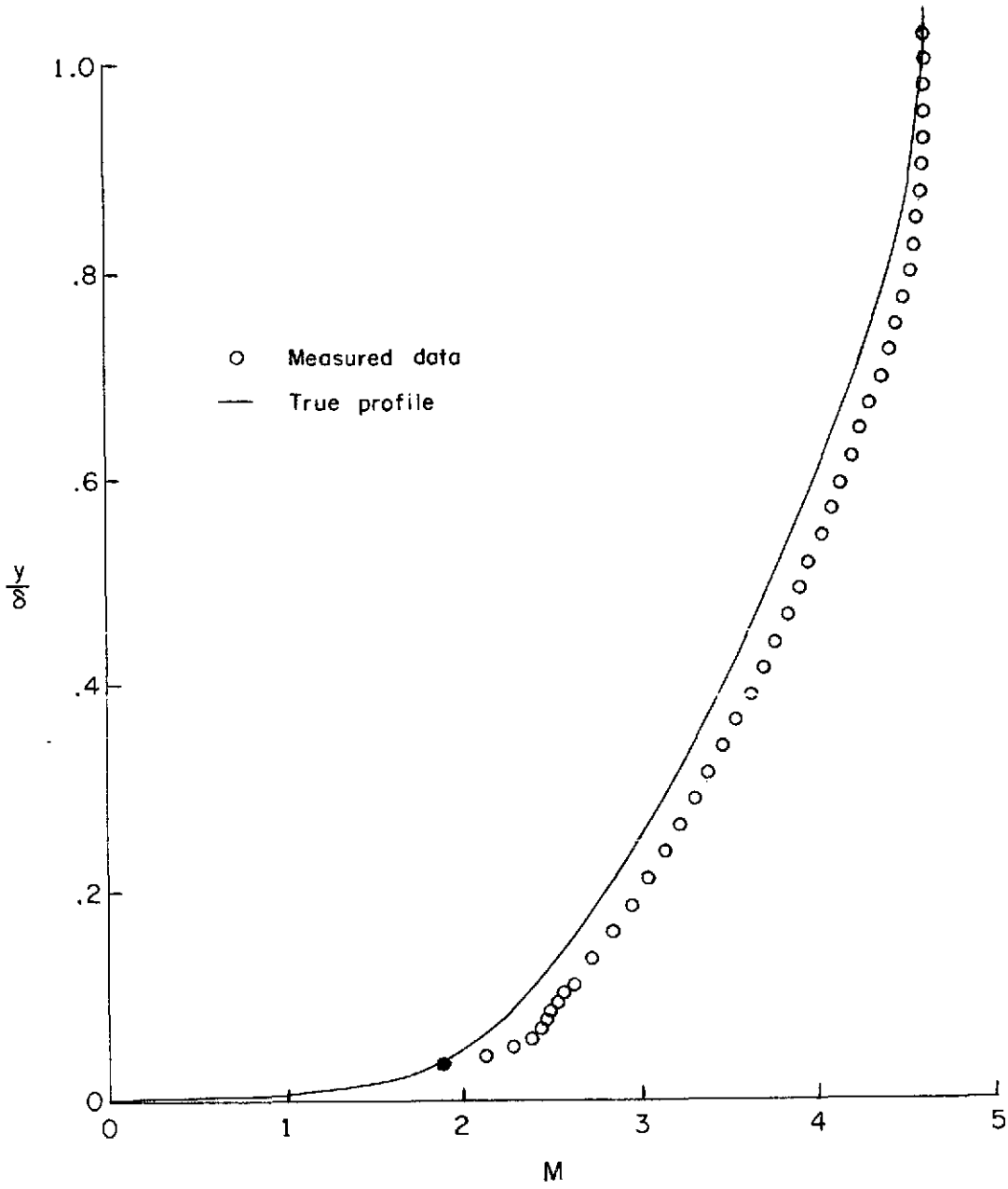

(d) $\frac{D}{\delta} = 0.068$. Solid symbol indicates wall contact point.

Figure 4.- Continued.

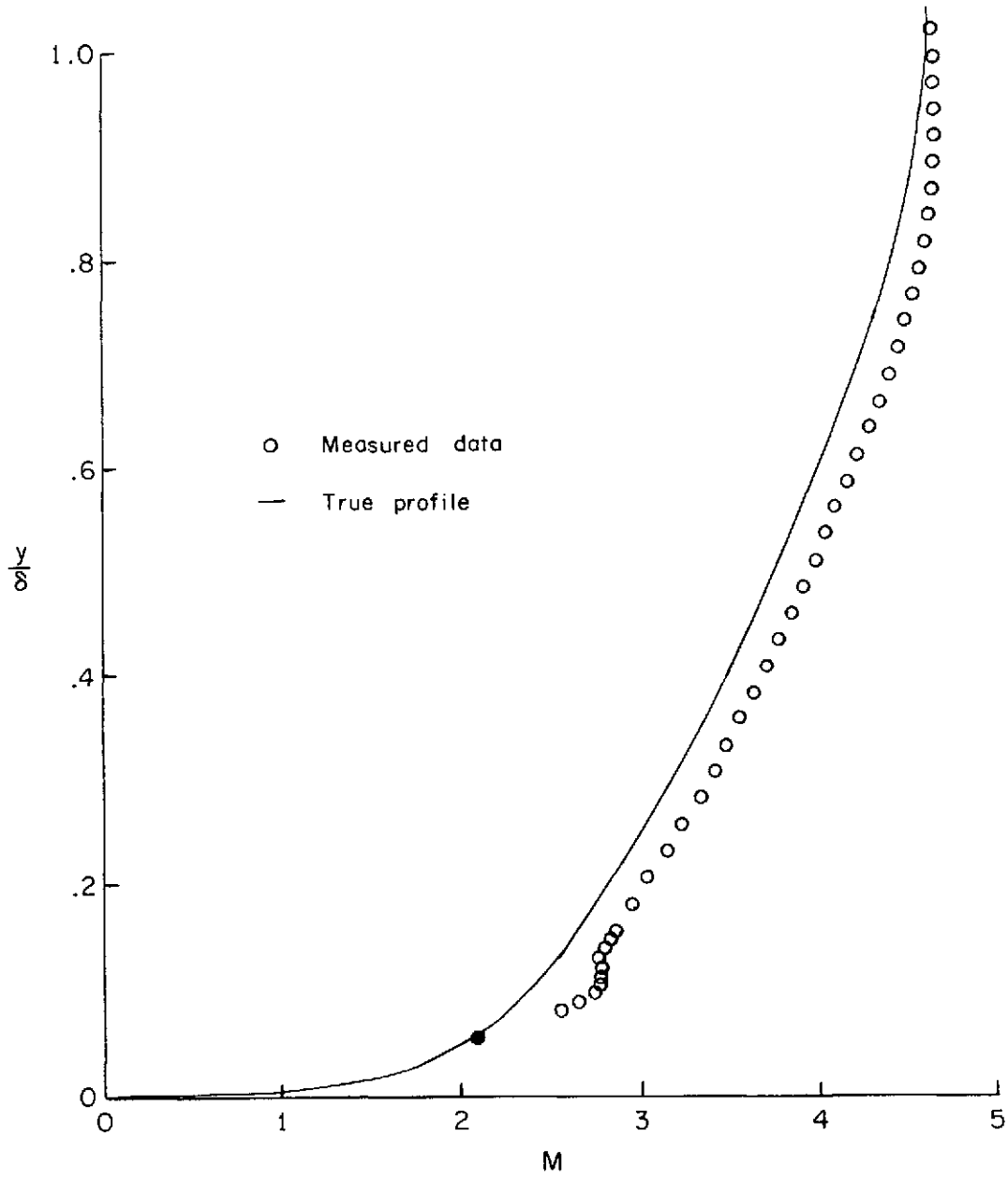

(e) $\frac{D}{\delta} = 0.119$. Solid symbol indicates wall contact point.

Figure 4.- Continued.

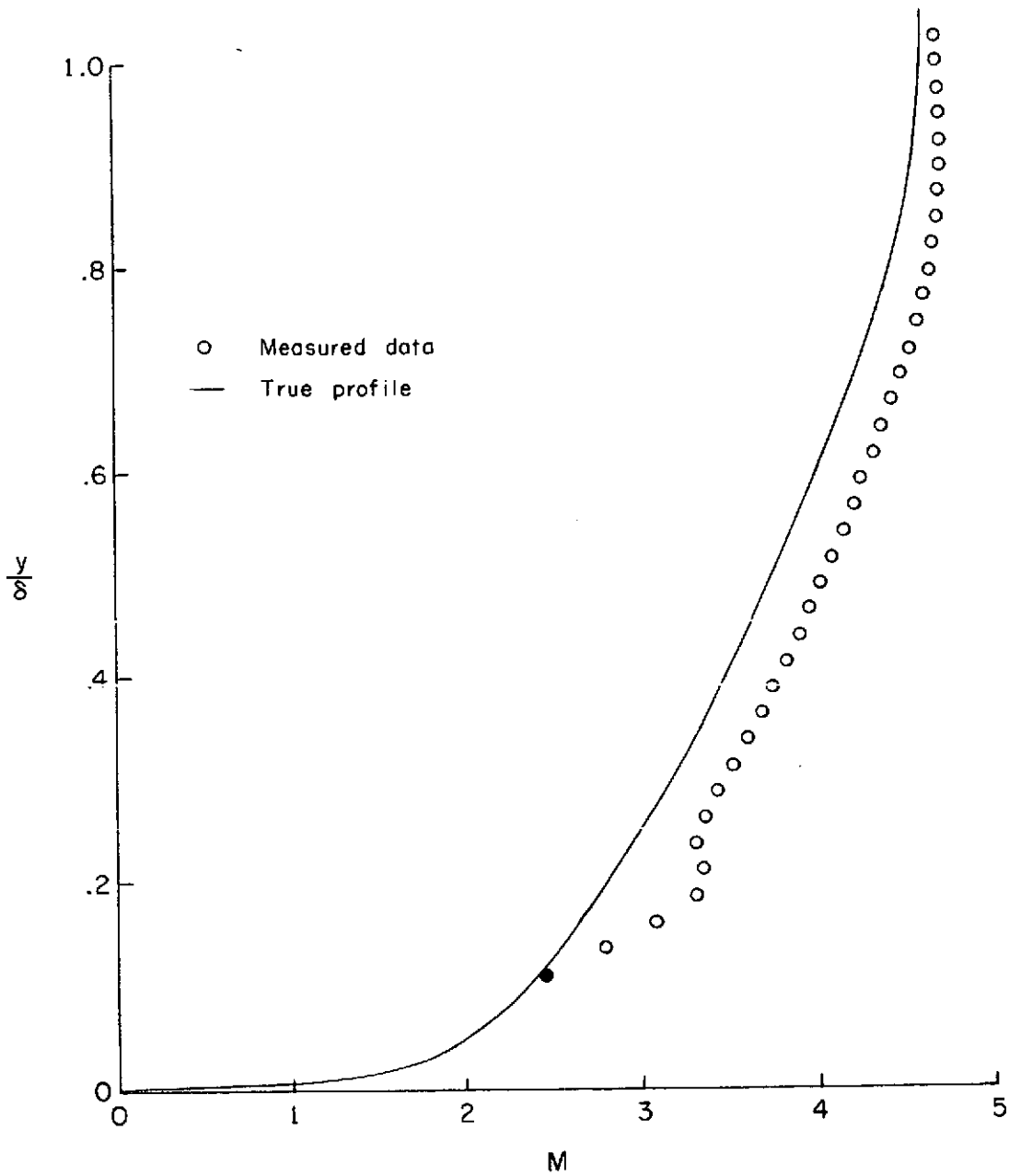

(f) $\frac{D}{\delta} = 0.169$. Solid symbol indicates wall contact point.

Figure 4.- Continued.

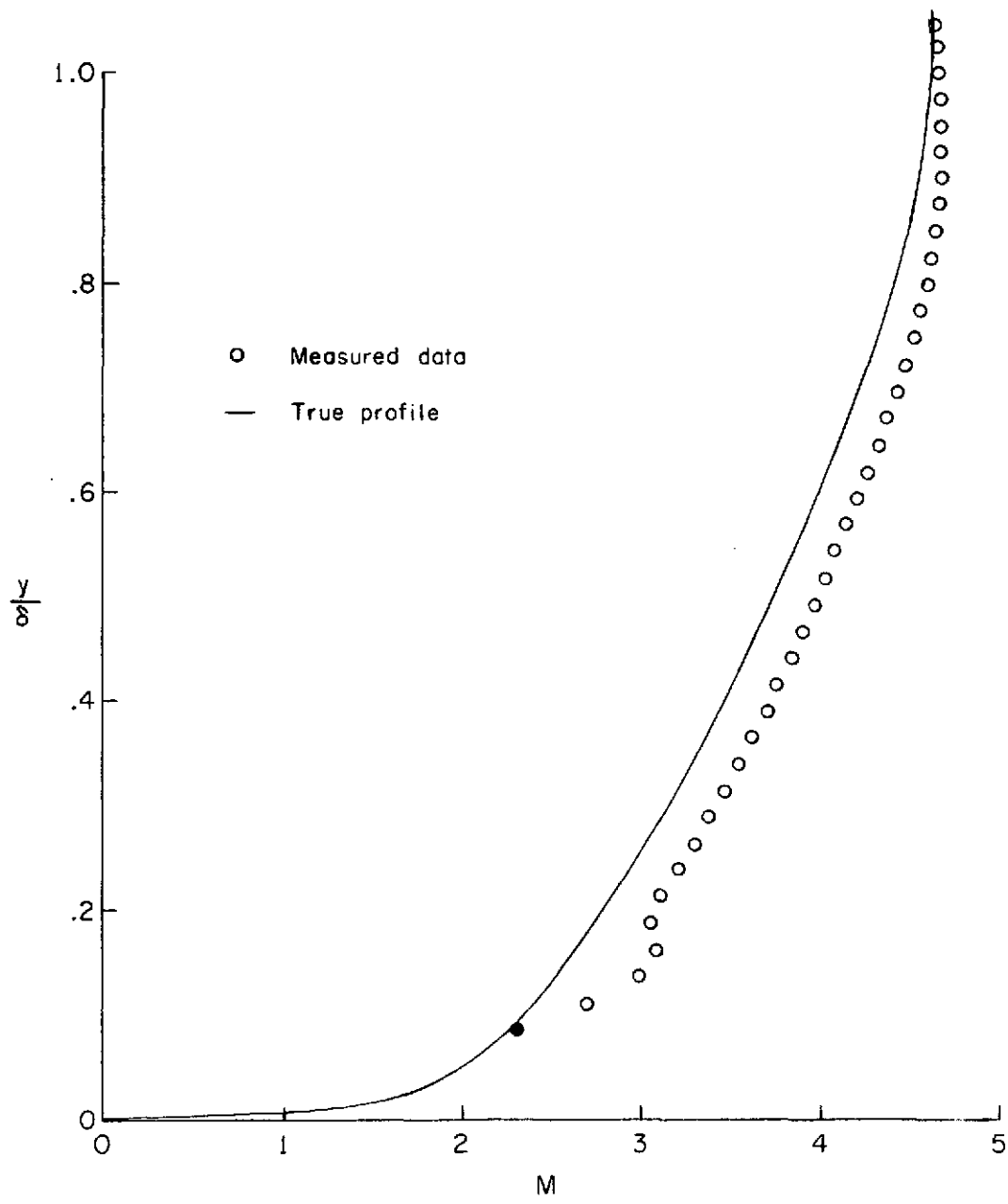

(g) $\frac{D}{\delta} = 0.220$. Solid symbol indicates wall contact point.

Figure 4.- Continued.

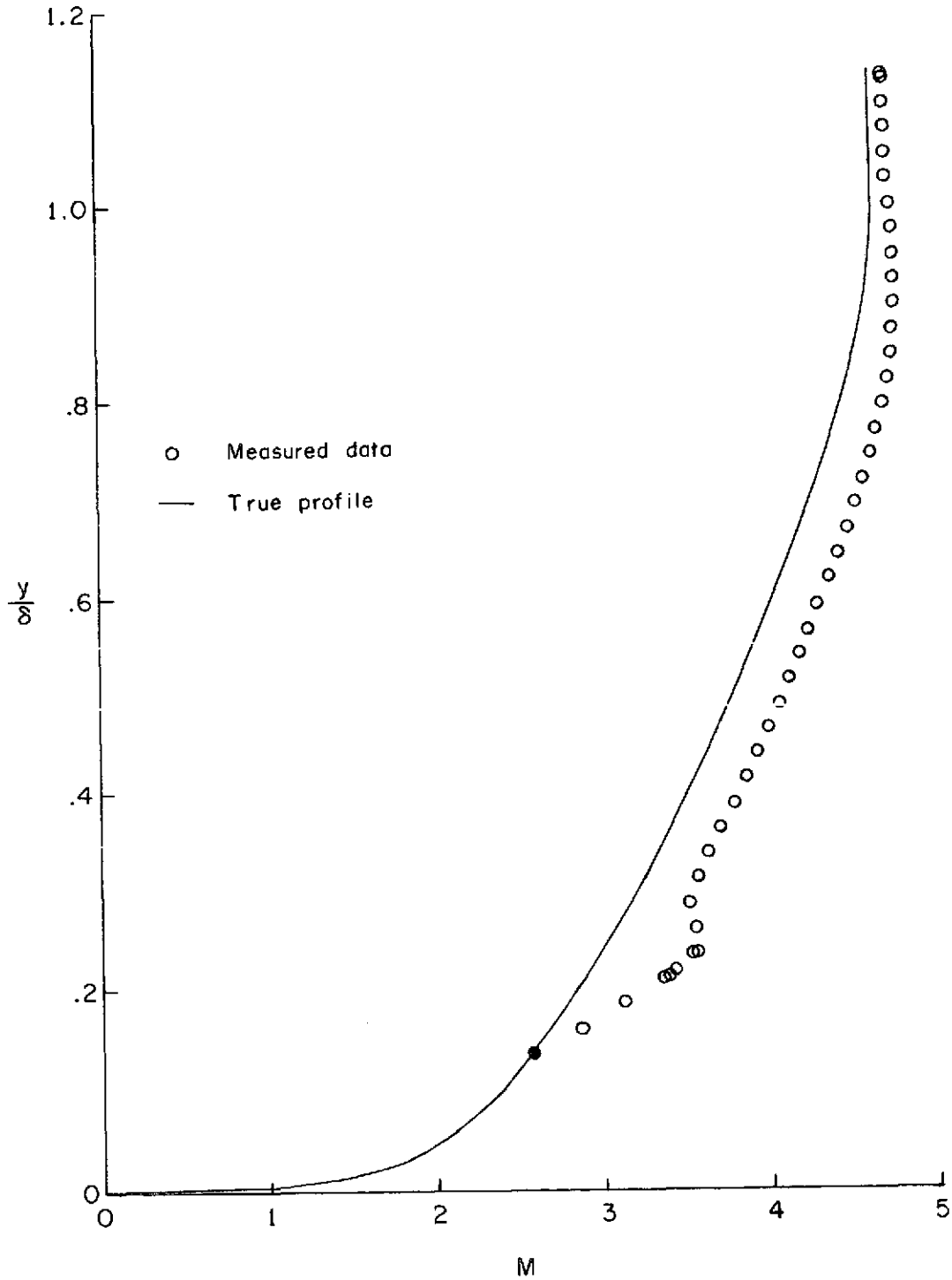

(h) $\frac{D}{\delta} = 0.271$. Solid symbol indicates wall contact point.

Figure 4.- Continued.

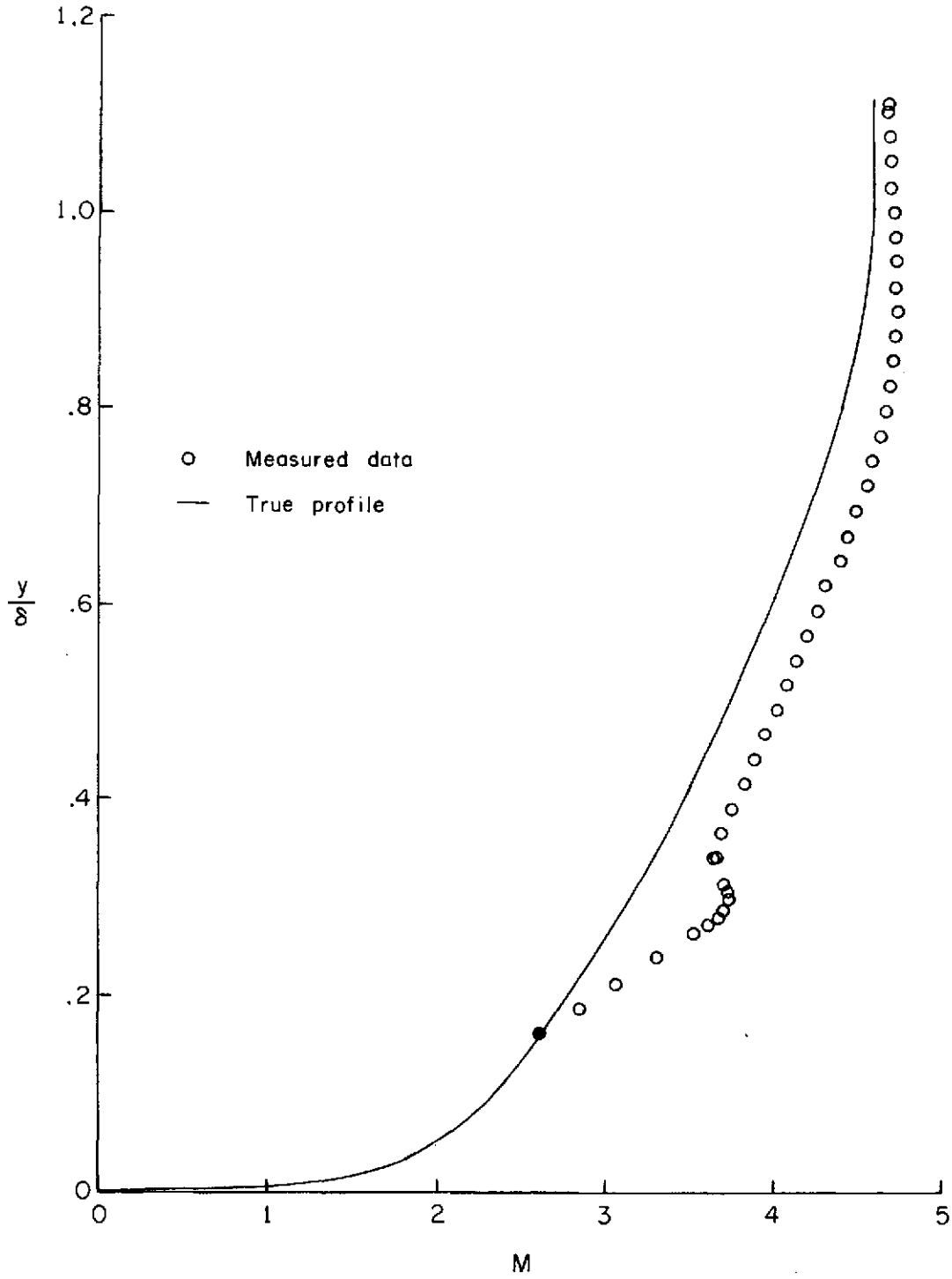

(i) $\frac{D}{\delta} = 0.322$. Solid symbol indicates wall contact point.

Figure 4.- Concluded.

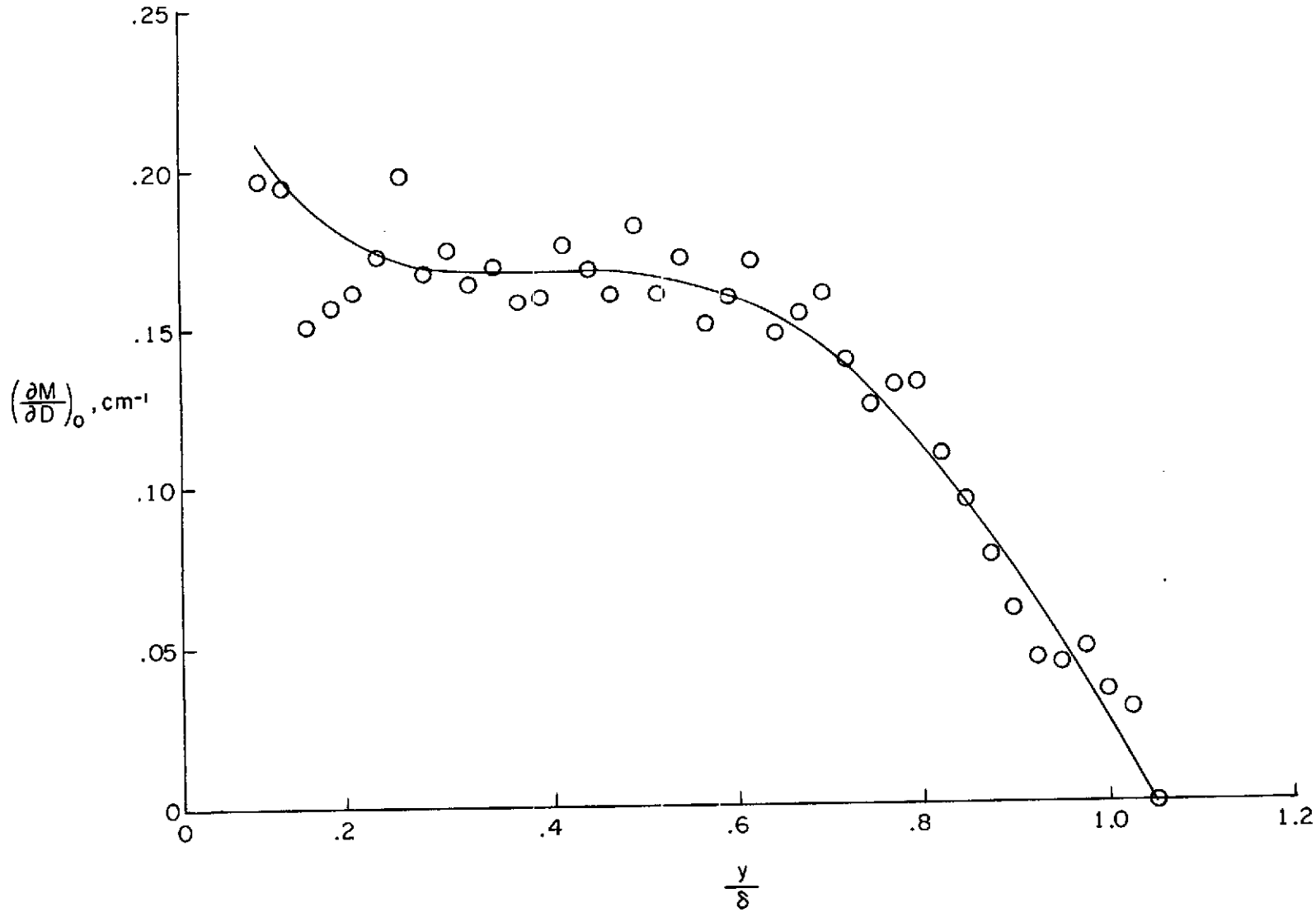

Figure 5.- Distribution of $\partial M/\partial D$ at $D = 0$.

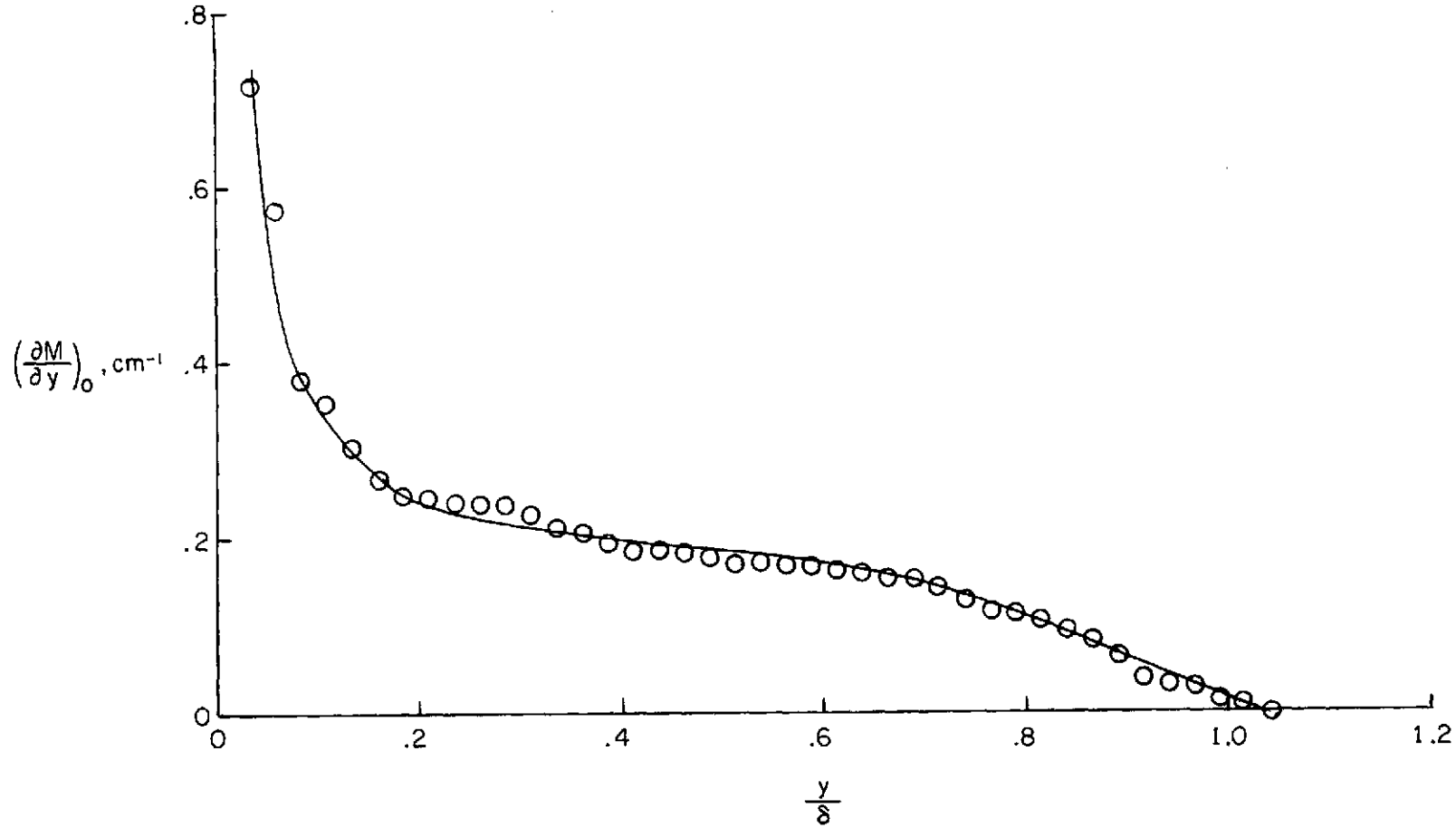

Figure 6.- Distribution of $\partial M/\partial y$ at $D = 0$.

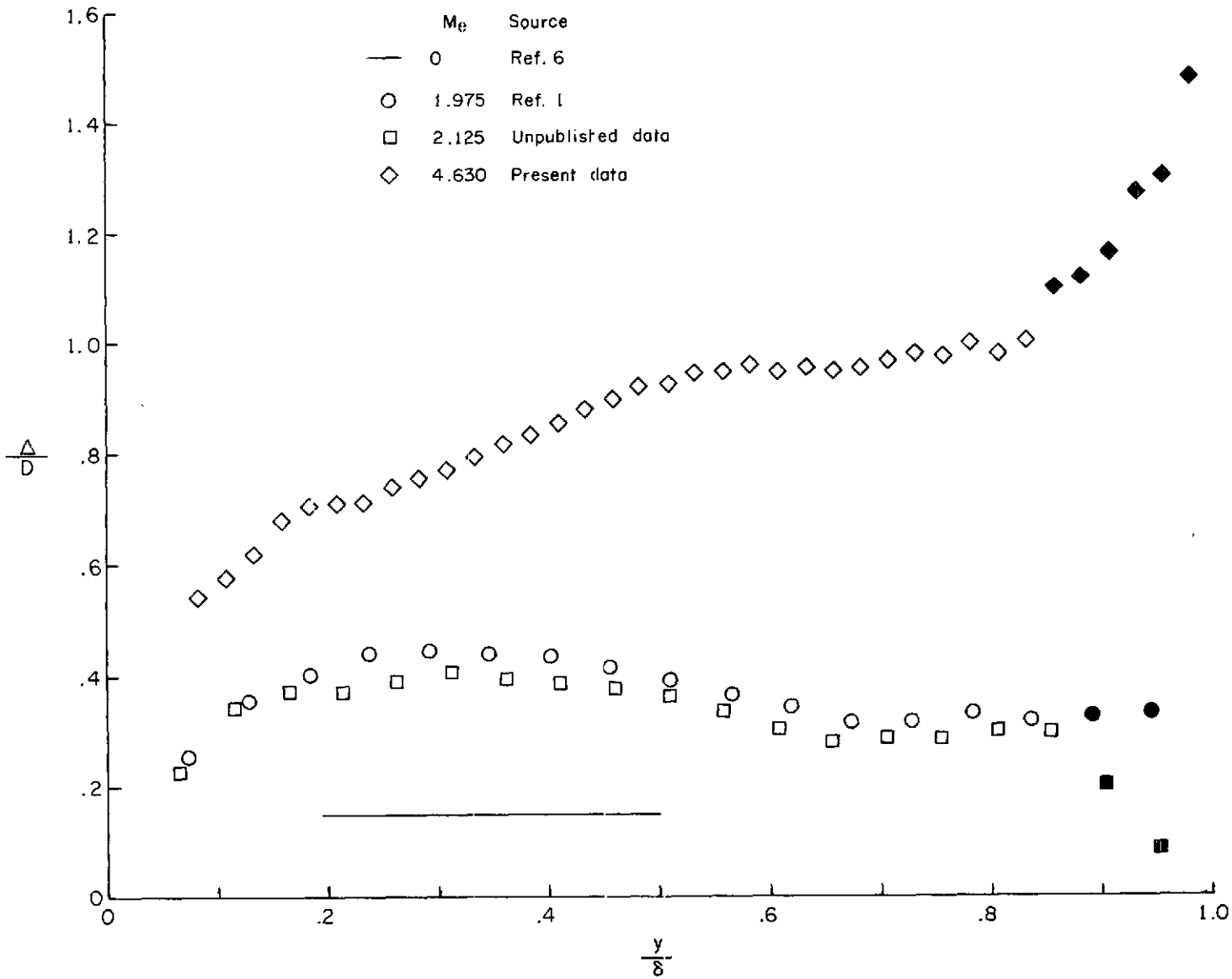

Figure 7.- Displacement distributions. Solid symbols indicate very inaccurate data.

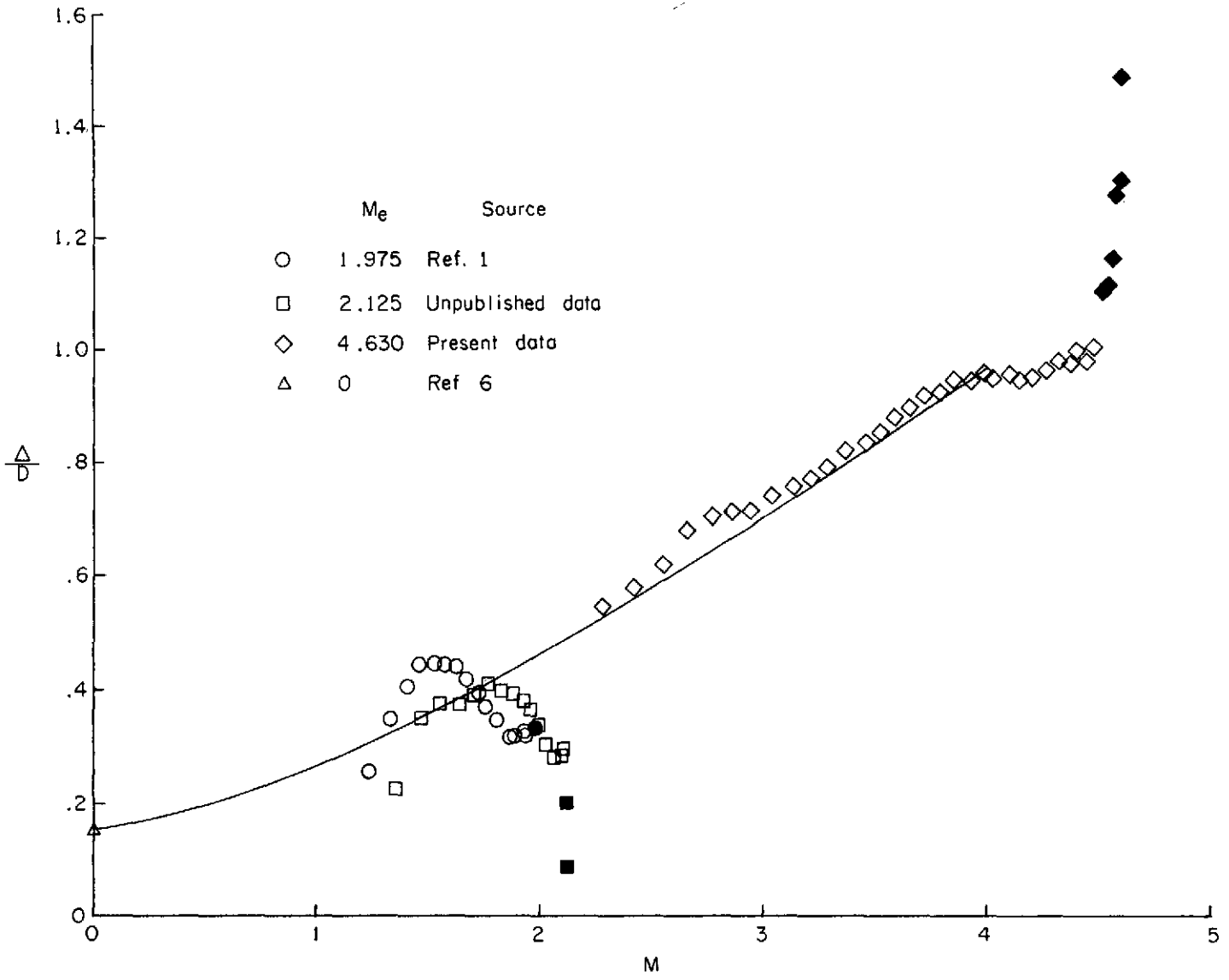

Figure 8.- Effect of Mach number on probe displacement. Solid symbols indicate very inaccurate data.